IOP Publishing Journal of Physics: Condensed Matter
J. Phys.: Condens. Matter **32** (2020) 275401 (12pp) https://doi.org/10.1088/1361-648X/ab7ba3

Hidden improper ferroelectric phases for design of antiferroelectrics

N V Ter-Oganessian and V P Sakhnenko

Institute of Physics, Southern Federal University, 194 Stachki Pr., 344090 Rostov-on-Don, Russia

E-mail: teroganesyan@sfedu.ru

Received 6 November 2019, revised 3 February 2020
Accepted for publication 2 March 2020
Published 7 April 2020

Abstract

Strong anomalous increase of the dielectric constant across a structural phase transition between two centrosymmetric phases, commonly observed in various crystals including prominent antiferroelectrics, is shown to originate from the hidden improper ferroelectric phases. In the vicinity of the phase transition double hysteresis loops of electric polarization vs electric field should be observed, which can be used for targeted design of antiferroelectric compounds. The suggested mechanism is illustrated by theoretical explanation of the recently discovered antiferroelectricity in the Ruddlesden–Popper compound $((CH_3)_2CHCH_2NH_3)_2CsPb_2Br_7$. Implications of the suggested models for the phase transition between the R and P phases in $NaNbO_3$ are discussed.

Keywords: improper ferroelectricity, dielectric constant, antiferroelectrics, $NaNbO_3$, Ruddlesden–Popper compounds

(Some figures may appear in colour only in the online journal)

1. Introduction

Since their discovery 100 years ago, ferroelectric materials have found numerous practical applications due to possession of electric polarization, which is one of the ferroic properties (the other two being magnetization and elastic deformation). The tensor nature of polarization leads to anomalies of dielectric constant at ferroelectric phase transitions. Such anomalies are usually the strongest at paraelectric–ferroelectric phase transitions, but can also be substantial at transitions between two ferroelectric phases.

In proper ferroelectrics the dielectric constant follows the Curie–Weiss behavior above and below the ferroelectric phase transition temperature and often reaches high values. In contrast, some crystals were found to disobey this temperature course showing minor anomalies at transitions to ferroelectric state, e.g., jumps of dielectric constant. Such crystal have been understood as improper ferroelectrics, in which the critical order parameter of the phase transition is not polarization, but some structural order parameter, whose condensation induces electric polarization in improper way [1, 2]. Examples of such behavior are ammonium Rochelle salt [3] and gadolinium molybdate [4]. The concept of improper ferroelectricity has gained renewed attention in the last two decades due to growth of interest in multiferroics—compounds, that combine at least two of the ferroic orders [5]. The so-called type-II multiferroics, in which magnetic ordering induces electric polarization, are essentially improper ferroelectric antiferromagnets [6].

In fact, ferroelectric compounds are relatively rare, and many of the technologically important ferroelectrics belong to the perovskite class, which is one of the richest crystallographic classes. Furthermore, perovskites are prone to structural distortions, however ferroelectric instability is found in relatively few compounds. Therefore, the continuing quest for new ferroelectric materials has led to understanding that combination of non-polar structural distortions or atomic orderings can result in occurrence of ferroelectricity [7–9]. On this basis the appearance of polarization has been understood in many compounds including, e.g., Ruddlesden–Popper phases [10], boracites [11], K_2SeO_4-type compounds [12, 13], Aurivillius [14, 15], and Dion–Jacobson [16] compounds.

In recent years antiferroelectric compounds have gained renewed interest due to potential practical applications in energy storage devices, for which the proximity of antiferroelectric and ferroelectric states is important [17]. In such compounds application of electric field beyond some

critical value results in appearance of electric polarization and double hysteresis loops, which are required for increased energy storage characteristics. Therefore, the combination of antiferroelectric (for example, $PbZrO_3$ and $PbSnO_3$) and ferroelectric (for example, $PbTiO_3$) materials is of the greatest interest. For this system the most significant results are obtained [18]. Interesting compounds from this point of view were also found on the basis of another antiferroelectric, $NaNbO_3$. Relatively small additions of $CaZrO_3$, $SrZrO_3$, or $CaHfO_3$ to $NaNbO_3$ (up to 5%–10%) lead to stabilization of the antiferroelectric phase and the appearance of double polarization loops [19–22]. $AgNbO_3$ also serves as the basis for observing such phenomena. Doping with Bi^{3+} ions in the *A* positions [23], W^{6+} [24] and Ta^{5+} [25] in the *B* positions leads to the stabilization of the antiferroelectric phase.

A number of crystalline compounds, that experience successive phase transitions with temperature, show anomalous increase of the dielectric constant across a phase transition between two centrosymmetric phases. As examples of such behavior one can point out the *Pbcm–Pmmn* transition in $NaNbO_3$ at $T_{AF} = 638$ K [26], the *Pbcm–Cmcm* transition in $AgNbO_3$ at $T_{AF} = 624$ K [27], the $P2_1/c$–$P2_1/c$ transition in betaine phosphate at $T_{AF} = 86$ K [28].

In this work, based on symmetrical and thermodynamical considerations, we develop two phenomenological models reproducing such behavior of dielectric constant at the first order phase transition between two centrosymmetric phases. The work is illustrated by the recent example of the Ruddlesden–Popper compound $((CH_3)_2CHCH_2NH_3)_2CsPb_2Br_7$, which shows significant dielectric constant anomaly at the paraelectric–antiferroelectric structural phase transition between two centrosymmetric phases [29] and appearance of double polarization loops below the phase transition temperature. In light of the obtained results we also discuss the phase transition between the R and P phases in $NaNbO_3$.

2. Phenomenological models

In this section based on symmetry and thermodynamics we consider two general phenomenological models, showing the above mentioned behavior of the dielectric constant (i.e., strong increase of ε) at the first order phase transition between centrosymmetric phases. The first model (model A) assumes the proximity of two phases induced by different order parameters transforming according to irreducible representations (IR) belonging to the same vector $\vec{k}$ of the reciprocal lattice. In the second model (model B) the first order phase transition is between the phases induced by a single two-component order parameter.

2.1. Model A

Let us write the expansion of thermodynamic potential Φ with respect to two one-component order parameters η and ξ, for which the symmetry allows interaction with electric polarization of the form $\eta\xi P$,

$$\Phi = \frac{a_1}{2}\eta^2 + \frac{a_2}{4}\eta^4 + \frac{b_1}{2}\xi^2 + \frac{b_2}{4}\xi^4 + \frac{\delta}{2}\eta^2\xi^2 + f\eta\xi P + \frac{1}{2\chi'}P^2 - EP, \tag{1}$$

where a_1, a_2, b_1, b_2, δ, and f are phenomenological coefficients, χ' is the dielectric susceptibility in the high symmetry phase, and E is electric field. The requirement of global stability of potential (1) is satisfied when $a_2 > 0$, $b_2 > 0$, and, in case $\delta - f^2\chi' < 0$, $a_2b_2 - (\delta - f^2\chi')^2 > 0$.

The equations of state correspond to the minimum of Φ and have the form

$$\begin{aligned}\frac{\partial\Phi}{\partial\eta} &= a_1\eta + a_2\eta^3 + f\xi P + \delta\eta\xi^2 = 0,\\ \frac{\partial\Phi}{\partial\xi} &= b_1\xi + b_2\xi^3 + f\eta P + \delta\eta^2\xi = 0,\\ \frac{\partial\Phi}{\partial P} &= \frac{P}{\chi'} + f\eta\xi - E = 0.\end{aligned} \tag{2}$$

The analysis of equation (2) reveals that at zero applied electric field ($E = 0$) apart from the high symmetry phase (HS), in which all the order parameters are zero, the following three phases are possible

$$\text{I.}\quad \eta^2 = -\frac{a_1}{a_2},\quad \xi = 0,\quad P = 0;$$

$$\text{II.}\quad \eta = 0,\quad \xi^2 = -\frac{b_1}{b_2},\quad P = 0;$$

$$\text{III.}\quad \eta^2 = -\frac{a_1b_2 - b_1\delta + b_1f^2\chi'}{a_2b_2 - (\delta - f^2\chi')^2},$$

$$\xi^2 = -\frac{a_2b_1 - a_1\delta + a_1f^2\chi'}{a_2b_2 - (\delta - f^2\chi')^2},$$

$$P = -f\chi'\eta\xi.$$

Thus, the phases I and II are paraelectric, whereas the phase III is improper ferroelectric.

Figures 1(a)–(c) show three possible schematic phase diagrams of model A valid for the following conditions imposed on the phenomenological coefficients: $a_2b_2 - (\delta - f^2\chi')^2 > 0$ and $\delta - f^2\chi' > 0$ [figure 1(a)], $\delta - f^2\chi' < 0$ [figure 1(b)], and $a_2b_2 - (\delta - f^2\chi')^2 < 0$ and $\delta - f^2\chi' > 0$ [figure 1(c)].

The lines 1 and 2 in figures 1(a)–(c) are given by equations

$$a_1 = \frac{a_2}{\delta - f^2\chi'}b_1,$$

$$a_1 = \frac{\delta - f^2\chi'}{b_2}b_1.$$

In the cases of figures 1(a) and (b) these are lines of second order phase transitions I–III and II–III, respectively, which are proper ferroelectric transitions, because, e.g., in the phase I when $\eta \neq 0$ there is a bilinear coupling between electric polarization and ξ meaning that ξ and P essentially have the same

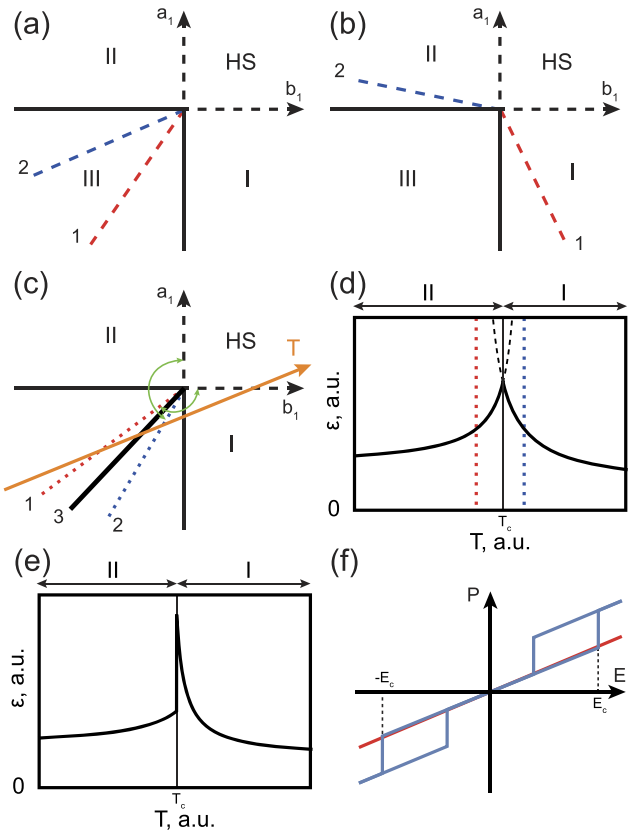

Figure 1. (a)–(c) Schematic phase diagrams for model A. The dashed lines are lines of second order phase transitions. The solid line 3 is a first order phase transition line. Dotted lines in (c) delimit regions of stability of phases as indicated by curved arrows. (d) Schematic temperature dependence of the dielectric constant across the first order phase transition I–II of figure (c). (e) Schematic temperature dependence of the dielectric constant across the first order phase transition I–II for the thermodynamic potential (5). (f) Dependencies of electric polarization on applied electric field $P(E)$ for the thermodynamic potential (5) far from and close to the I–II phase transition shown by the red and blue lines, respectively.

symmetry. Therefore, these phase transitions are accompanied by divergence of the dielectric susceptibility

$$\chi = \frac{\mathrm{d}P}{\mathrm{d}E}.$$

In case $a_2b_2 - (\delta - f^2\chi')^2 < 0$ and $\delta - f^2\chi' > 0$, which corresponds to figure 1(c), the improper ferroelectric phase III is unstable and is, thus, absent from the phase diagram. In figure 1(c) the lines 1 and 2 delimit the regions of stability of the phases I and II, respectively, as indicated by curved arrows. Therefore, there is a direct first order phase transition between the phases I and II at line 3 given by equation

$$a_1 = \sqrt{\frac{a_2}{b_2}}b_1.$$

In the low symmetry phases one can calculate the dielectric susceptibility χ, which in the phases I and II results in

$$\chi_{\mathrm{I}} = \chi' - \frac{a_1 f^2 \chi'^2}{a_2 b_1 - a_1\delta + a_1 f^2 \chi'}, \tag{3}$$

$$\chi_{\mathrm{II}} = \chi' - \frac{b_1 f^2 \chi'^2}{a_1 b_2 - b_1\delta + b_1 f^2 \chi'}, \tag{4}$$

respectively. One can note that χ_{I} and χ_{II} diverge at the lines 1 and 2, which confirms the proper ferroelectric nature of the phase transitions I–III and II–III in figures 1(a) and (b). In the case of figure 1(c), i.e., when the ferroelectric phase III is unstable, the dielectric susceptibilities (3) and (4) still diverge at lines 1 and 2, respectively, which restrict the regions of stability of phases I and II, however the first order phase transition occurs at line 3. Figure 1(c) also shows a possible thermodynamic path, i.e., a temperature axis T, along which the behavior of the dielectric constant is shown in figure 1(d). One can find that despite the absence of ferroelectric phase in the phase diagram the dielectric constant experiences a strong increase close to the first order phase transition between two centrosymmetric phases I and II occurring at temperature T_{c}. The narrower is the region of simultaneous stability of both phases I and II between the lines 1 and 2, the sharper is the maximum of ε at T_{c}.

It is interesting to note also, that in the present model, in which the expansion of thermodynamic potential (1) is truncated at terms of fourth order with respect to η and ξ, the dielectric constant is continuous across the first order phase transition I–II as shown in figure 1(d), however inclusion of higher order terms into consideration should result in appearance of a jump of the dielectric constant at this phase transition. In order to describe this behavior we extend the thermodynamic potential (1) to include higher order terms truncating it at sixth power with respect to η and ξ and omitting higher order interactions between them. The corresponding thermodynamic potential has the form

$$\Phi = \frac{a_1}{2}\eta^2 + \frac{a_2}{4}\eta^4 + \frac{a_3}{6}\eta^6 + \frac{b_1}{2}\xi^2 + \frac{b_2}{4}\xi^4 + \frac{b_3}{6}\xi^6 + \frac{\delta}{2}\eta^2\xi^2 + f\eta\xi P + \frac{1}{2\chi'}P^2 - EP, \tag{5}$$

where additional phenomenological coefficients a_3 and b_3 are used. The thermodynamic potential (5) is much more difficult to analyze analytically than (1). Therefore, here we provide a sample numerical calculation. Taking the values of phenomenological coefficients $a_2 = -1$, $a_3 = 4.3$, $b_2 = 0.2$, $b_3 = 4.4$, $\delta = 3$, $f = 1$, $\chi' = 0.1$, we obtain the dielectric constant behavior across the first order phase transition between the phases I and II as shown in figure 1(e).

The closeness of the ferroelectric phase III on the thermodynamic path results in appearance of double loops of electric polarization vs electric field $P(E)$ close to and below T_{c}, which are characteristic of antiferroelectrics. Application of small electric field in both phases I and II results in appearance of small P as in ordinary paraelectric. Further increase of electric field above some critical field E_{c} should result in a first order field-induced phase transition into phase III with higher electric polarization. Such behavior, similar to the description of the jump of ε across the I–II phase transition, can also be described by thermodynamic potential expansion to powers

higher than 4. For the thermodynamic potential (5) and the values of phenomenological coefficients given above the double hysteresis loop $P(E)$ is shown in figure 1(f).

2.2. Model B

In this model we consider phase transitions with respect to a single two-component order parameter (η_1, η_2) that allows interaction with polarization of the form $\eta_1\eta_2\left(\eta_1^2 - \eta_2^2\right)P$. In fact, such examples are numerous and in many cases there are symmetry arguments for the existence of such interactions for certain order parameters [6]. The thermodynamic potential expansion can be written in the form

$$\Phi = \frac{a_1}{2}\left(\eta_1^2 + \eta_2^2\right) + \frac{a_2}{4}\left(\eta_1^4 + \eta_2^4\right) + \frac{a_3}{4}\left(\eta_1^2 + \eta_2^2\right)^2 + f\eta_1\eta_2\left(\eta_1^2 - \eta_2^2\right)P + \frac{1}{2\chi'}P^2 - EP, \tag{6}$$

where a_1, a_2, a_3, and f are phenomenological coefficients, χ' is the dielectric susceptibility in the high symmetry phase, and E is electric field. The requirement of global stability of potential (6) is satisfied when $a_2 + a_3 > 0$.

The equations of state corresponding to the minimum of Φ have the form

$$\begin{aligned}
\frac{\partial\Phi}{\partial\eta_1} &= a_1\eta_1 + a_2\eta_1^3 + 2f\eta_1^2\eta_2P + f\eta_2(\eta_1^2 - \eta_2^2)P \\
&\quad + a_3\eta_1(\eta_1^2 + \eta_2^2) = 0, \\
\frac{\partial\Phi}{\partial\eta_2} &= a_1\eta_2 + a_2\eta_2^3 - 2f\eta_1\eta_2^2P + f\eta_1(\eta_1^2 - \eta_2^2)P \\
&\quad + a_3\eta_2(\eta_1^2 + \eta_2^2) = 0, \\
\frac{\partial\Phi}{\partial P} &= \frac{P}{\chi'} + f\eta_1\eta_2(\eta_1^2 - \eta_2^2) - E = 0.
\end{aligned} \tag{7}$$

The analysis of equation (7) reveals that at zero applied electric field ($E = 0$) apart from the high symmetry phase (HS), in which all the order parameters are zero, the following three phases are possible

$$\begin{aligned}
&\text{I.} \quad \eta_1^2 = \eta_2^2 = -\frac{a_1}{a_2 + 2a_3}, \quad P = 0; \\
&\text{II.} \quad \eta_1^2 = -\frac{a_1}{a_2 + a_3}, \quad \eta_2 = 0, \quad P = 0; \\
&\text{III.} \quad \eta_1 \neq 0, \quad \eta_2 \neq 0, \quad |\eta_1| \neq |\eta_2|, \quad P \neq 0.
\end{aligned}$$

Thus, the phases I and II are paraelectric, whereas the phase III is an improper ferroelectric phase. Schematic phase diagram for model B is shown in figure 2(a). All phase transitions HS-I, HS-II, I–III, and II–III are of second order. It has to be noted, that phase III borders with the high symmetry phase at a single point $a_1 = a_2 = 0$. The width of the region of phase III in the phase diagram grows as $\sqrt{a_2}$ near this point. Therefore, the region of stability of phase III is very narrow. The phase transitions I–III and II–III are proper ferroelectric, which results in divergence of the dielectric constant at lines 1 and 2 in figure 2(a).

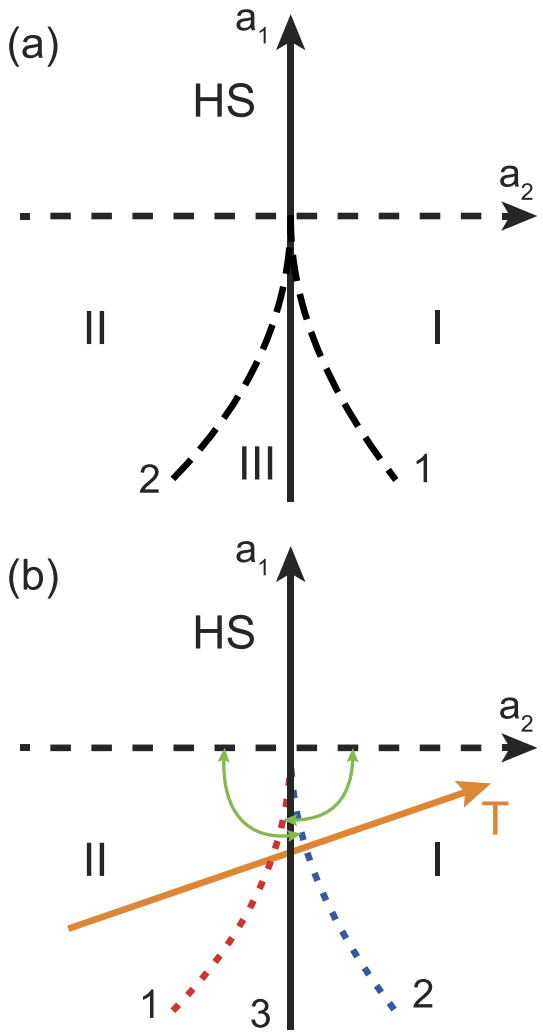

Figure 2. (a) Schematic phase diagram for model B. The dashed lines are lines of second order phase transitions. (b) Schematic phase diagram for model B in the case when phase III is not stable. Dotted lines 1 and 2 delimit the regions of stability of phases I and II as shown by the curved arrows. The dashed line is a second order phase transition line. The solid line 3 is a first order phase transition line.

In this model we for simplicity truncated the expansion of thermodynamic potential (6) at the fourth power with respect to the order parameter (η_1, η_2). However, it can be shown that proper description of the phase III requires expansion up to the eighth power. Depending on the coefficients at the higher order terms two cases are possible. The first one is similar to that shown in figure 2(a) with narrow region of stability of phase III between the phases I and II. In the second case there is a direct first order phase transition I–II, whereas phase III is absent from the phase diagram. The corresponding phase diagram is shown in figure 2(b). In this case the dotted lines 1 and 2 also delimit the regions of stability of the phases I and II, respectively. Furthermore, it can be found that the behavior of the dielectric constant across the I–II phase transition along the thermodynamic path shown in figure 2(b) is similar to that in figure 1(d). Therefore, ε experiences considerable increase at the phase transition between two nonferroelectric phases I and II.

Table 1. The lattice parameters and atomic positions in the HT phase of $(i\text{-BA})_2CsPb_2Br_7$ according to the experimental data [29] (left panel) and the same parameters, which result in higher symmetry paraphase structure (right panel).

Cmce (experimental)					*Cmce* (symmetrized)				
$a = 39.75$ Å, $b = 8.2718$ Å, $c = 8.2733$ Å					$a = 39.75$ Å, $b = c = 8.2726$ Å				
Atom	x	y	z	Occ.	Atom	x	y	z	Occ.
Pb	0.4244	0.0	0.5	1.0	Pb	0.4244	0.0	0.5	1.0
Br_1	0.4254	0.3018	0.6985	1.0	Br_1	0.4254	0.25	0.75	1.0
Br_2	0.5	0.0	0.5	1.0	Br_2	0.5	0.0	0.5	1.0
Br_3	0.3509	0.0	0.5	1.0	Br_3	0.3509	0.0	0.5	1.0
Cs	0.5	0.5	0.5	1.0	Cs	0.5	0.5	0.5	1.0
C_1	0.3375	0.5	0.5	1.0	C_1	0.3375	0.5	0.5	1.0
C_2	0.3001	0.5	0.5	1.0	C_2	0.3001	0.5	0.5	1.0
C_3	0.2886	0.3370	0.4480	0.5	C_3	0.2884	0.3300	0.5	0.5
C_4	0.2882	0.5200	0.6680	0.5	C_4	0.2884	0.5	0.6700	0.5
					N_1	0.3662	0.4229	0.4229	0.25
N	0.3662	0.4280	0.4180	0.5	N_2	0.3662	0.4229	0.5771	0.25
					H_{1A1}	0.3854	0.4631	0.4631	0.25
H_{1A}	0.3854	0.4660	0.4604	0.5	H_{1A2}	0.3854	0.4631	0.5369	0.25
					H_{1B1}	0.3653	0.3160	0.4414	0.25
H_{1B}	0.3653	0.3201	0.4296	0.5	H_{1B2}	0.3653	0.4414	0.684	0.25
					H_{1C1}	0.3653	0.4414	0.3160	0.25
H_{1C}	0.3653	0.4531	0.3118	0.5	H_{1C2}	0.3653	0.3160	0.5586	0.25
H_{1D}	0.3424	0.4756	0.6110	0.5	H_{1D}	0.3424	0.5	0.6136	0.5
H_{1E}	0.3424	0.6131	0.4891	0.5	H_{1E}	0.3424	0.3864	0.5	0.5
					H_{2A1}	0.292	0.5772	0.4228	0.25
H_{2A}	0.2920	0.5880	0.4353	0.5	H_{2A2}	0.292	0.4228	0.4228	0.25
H_{3A}	0.2644	0.3344	0.4471	0.5	H_{3A}	0.2643	0.3262	0.5	0.5
H_{3B}	0.2969	0.3268	0.3399	0.5	H_{3B}	0.2969	0.2758	0.4058	0.5
H_{3C}	0.2969	0.2495	0.5129	0.5	H_{3C}	0.2969	0.2758	0.5942	0.5
H_{4A}	0.2959	0.6213	0.7109	0.5	H_{4A}	0.2969	0.5942	0.7242	0.5
H_{4B}	0.2641	0.5174	0.6694	0.5	H_{4B}	0.2643	0.5	0.6738	0.5
H_{4C}	0.2968	0.4331	0.7328	0.5	H_{4C}	0.2969	0.4058	0.7242	0.5

3. Phase transition in $(i\text{-BA})_2CsPb_2Br_7$

The hybrid organic-inorganic layered Ruddlesden–Popper (RP) perovskite $(i\text{-BA})_2CsPb_2Br_7$, where *i*-BA is isobutylammonium $((CH_3)_2CHCH_2NH_3)^+$, shows a structural phase transition at $T_c = 353$ K between two centrosymmetric phases, which is accompanied by a remarkable maximum of the dielectric constant [29]. The high (HT) and the low (LT) temperature phases have the symmetries *Cmce* and *Pmnb*, respectively, and are characterized by antiparallel displacements of ions. Below T_c double loops of electric polarization vs electric field (*P*–*E*) are observed, with electric polarization reaching 6.3 μC cm^{-2}, which confirms the antiferroelectric nature of the LT phase.

The observed *Cmce*–*Pmnb* phase transition between two centrosymmetric phases can not explain the accompanying pronounced maximum of the dielectric constant. The highest crystal lattice symmetry attained by RP layered perovskite compounds is $I4/mmm$. This structure can be thought of as the praphase for all RP compounds, despite the fact that some of them do not experience the highest possible symmetry, which is the case of organic–inorganic $(i\text{-BA})_2CsPb_2Br_7$, that is stable only up to 520 K [29]. By praphase we mean the most symmetrical structure of the given compound, that can be attained by displacement of atoms toward the positions of higher symmetry or by redistribution of atoms within the set of equivalent crystallographical positions assumed for the higher symmetry state. The praphase concept is used in the theory of phase transitions for, e.g. the description of reconstructive phase transitions [30]. Such phase transitions occur between phases that have no group-subgroup relation. However, one may find a crystal structure (the praphase) that is a common supergroup of the above mentioned phases, between which the reconstructive phase transition occurs. The latter can then be described as the phase transition between two subphases of the praphase. Such approach has been successfully applied in the description of, e.g., phase transitions in multiferroics [31, 32]. One of the advantages of the praphase approach is the account of latent pseudosymmetries existing in the crystal structure, which provides valuable information about the nature of

Table 2. The lattice parameters and atomic positions of the tetragonal praphase structure of $(i\text{-BA})_2CsPb_2Br_7$.

	$I4/mmm$			
	$a = 5.8495$ Å, $c = 39.75$ Å			
Atom	x	y	z	Occ.
Pb	0.0	0.0	0.0756	1.0
Br_1	0.0	0.5	0.4254	1.0
Br_2	0.0	0.0	0.0	1.0
Br_3	0.0	0.0	0.1491	1.0
Cs	0.0	0.0	0.5	1.0
C_1	0.0	0.0	0.6625	1.0
C_2	0.0	0.0	0.6999	1.0
C_3	0.8300	0.8300	0.7116	0.5
N	0.0	0.1540	0.6338	0.25
H_{1A}	0.0	0.0738	0.6146	0.25
H_{1B}	0.7574	0.1254	0.3653	0.25
H_{1C}	0.1136	0.1136	0.3424	0.5
H_2	0.0	0.8456	0.292	0.25
H_3	0.8262	0.8262	0.7357	0.5
H_4	0.6816	0.1300	0.2969	0.5

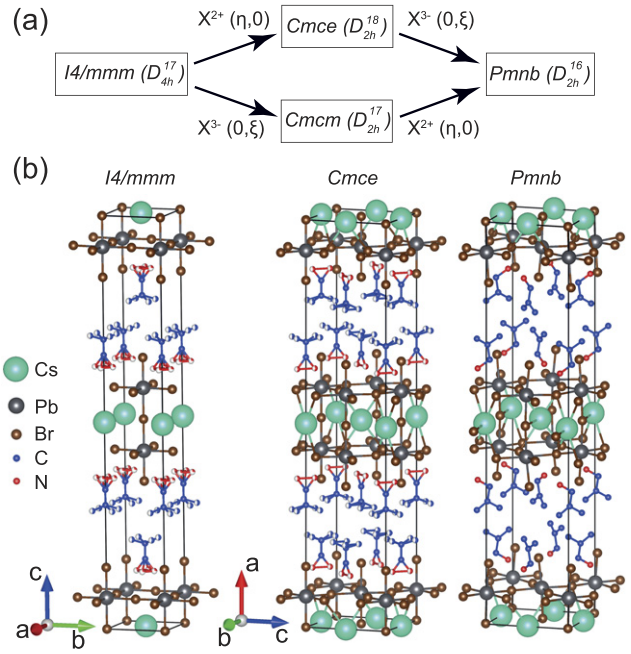

Figure 3. (a) Relation between the space groups of the praphase and the low symmetry structures. (b) Crystal structures in the $I4/mmm$, *Cmce*, and *Pmnb* phases. Hydrogen atoms are omitted for clarity.

various instabilities occurring in the crystal. As a result a symmetrically substantiated thermodynamic potential can be constructed and used for thermodynamic analysis of the whole set of phase transitions including phase transitions between low-symmetry phases not connected by a group–subgroup relation. Therefore, all the phase transitions in RP compounds can be described starting from the tetragonal praphase. To this end one has to find the lattice distortions resulting in lowering the praphase symmetry to those of HT and LT phases.

3.1. Symmetrization to the $I4/mmm$ structure

Small atomic displacements and lattice deformations of the HT phase result in appearance of high symmetry $I4/mmm$ structure characteristic for RP family of compounds. The corresponding changes are given in table 1. The atomic positions have to be symmetrized in order to restore the higher symmetry of the praphase structure. In the HT phase each of the $i\text{-BA}^+$ cations is disordered between two configurations, whereas at the HT–LT phase transition the organic cations become ordered. Therefore, the transition at T_c pertains to the order-disorder phase transition, however atomic displacements also occur. In order to restore tetragonal symmetry with the four-fold axis one has to introduce additional positions and alter the occupational parameters for nitrogen and hydrogen ions, which participate in the order-disorder process. This is also reflected in table 1. It can be found that the structure symmetrized in such a way has a tetragonal symmetry $I4/mmm$ and the respective crystallographic parameters are given in table 2.

Analysis of the mechanical and occupational representations for the high symmetry $I4/mmm$ tetragonal structure shows that the hypothetical phase transition to the *Cmce* phase is described by IR X^{2+}. The phase transition at T_c is connected with additional condensation of IRs X^{3-} and M^{5-}. As argued below, only X^{2+} and X^{3-} out of these three IRs can be considered as primary instabilities occurring in $(i\text{-BA})_2CsPb_2Br_7$, whereas M^{5-} is induced as a secondary order parameter. The relationship between the praphase and the low symmetry HT and LT structures is shown in figure 3(a), whereas figure 3(b) gives the crystal structures for the praphase, HT, and LT phases.

3.2. Phenomenological model

The structural phase transition in $(i\text{-BA})_2CsPb_2Br_7$ and the occurring anomaly of the dielectric constant can be described by a phenomenological model accounting for the two primary instabilities of the parent praphase structure in the X-point of the Brillouin zone. The expansion of thermodynamic potential with respect to the order parameters (η_1, η_2) and (ξ_1, ξ_2), transforming according to IRs X^{2+} and X^{3-}, respectively, and taking into account electric polarization can be written as

$$\begin{aligned}\Phi = {} & \frac{a_1}{2}\left(\eta_1^2+\eta_2^2\right)+\frac{a_2}{4}\left(\eta_1^4+\eta_2^4\right)+\frac{a_3}{4}\left(\eta_1^2+\eta_2^2\right)^2 \\ & +\frac{A_1}{2}\left(\xi_1^2+\xi_2^2\right)+\frac{A_2}{4}\left(\xi_1^4+\xi_2^4\right)+\frac{A_3}{4}\left(\xi_1^2+\xi_2^2\right)^2 \\ & +\delta_1\left(\eta_1^2\xi_1^2+\eta_2^2\xi_2^2\right)+\delta_2\left(\eta_1^2+\eta_2^2\right)\left(\xi_1^2+\xi_2^2\right) \\ & +\frac{1}{2\chi'}\left(P_x^2+P_y^2\right)+fI-\left(E_xP_x+E_yP_y\right), \end{aligned} \tag{8}$$

where

$$I = \eta_1\xi_1\left(P_x+P_y\right)+\eta_2\xi_2\left(P_x-P_y\right), \tag{9}$$

a_1, a_2, a_3, A_1, A_2, A_3, δ_1, δ_2, and f are phenomenological coefficients, and χ' is the dielectric susceptibility of $(i\text{-BA})_2CsPb_2Br_7$ in the praphase structure in the xy plane. Here we assume the coordinate axes x, y, and z along the crystallographic axes a, b, and c of the tetragonal praphase structure, respectively. One should note the existence of invariant I in the expansion (8), which is qualitatively similar to the invariant $\eta\xi P$ considered in the model A (see section 2.1), although is more complex due to the two-dimensional nature of order parameters (OP) (η_1, η_2) and (ξ_1, ξ_2).

Invariant I implies that some of the phases induced by simultaneous condensation of X^{2+} and X^{3-} are improper ferroelectric, namely those, in which either $\eta_1\xi_1$ or $\eta_2\xi_2$ or both have nonzero values. In the HT phase only the OP (η_1, η_2) is nonzero with the value $(\eta, 0)$, whereas in the LT phase the OPs have values $(\eta, 0)$ and $(0, \xi)$, respectively, implying that $I = 0$ and the phase is centrosymmetric.

The condensation at T_c of the secondary order parameter (γ_1, γ_2) transforming by M^{5-} is due to the presence of invariant

$$J = \eta_1\xi_2\gamma_1 - \eta_2\xi_1\gamma_2.$$

In the HT phase J reduces to $\eta\xi_2\gamma_1$ and, thus, ξ_2 and γ_1 have the same symmetry and simultaneously appear at T_c.

In the HT and LT phases both OPs (η_1, η_2) and (ξ_1, ξ_2) are characterized by at most one nonzero component, which is possible if the conditions $a_2 < 0$, $a_2 + a_3 > 0$, $A_2 < 0$, and $A_2 + A_3 > 0$ hold and we further assume their validity to simplify our phenomenological treatment. The stable phases then are

I. $$\eta_1^2 = -\frac{a_1}{a_2 + a_3}, \quad \eta_2 = \xi_1 = \xi_2 = 0, \quad P_x = P_y = 0;$$

I′. $$\xi_1^2 = -\frac{A_1}{A_2 + A_3}, \quad \eta_1 = \eta_2 = \xi_2 = 0, \quad P_x = P_y = 0;$$

II. $$\eta_1^2 = -\frac{a_1(A_2 + A_3) - 2A_1\delta_2}{(a_2 + a_3)(A_2 + A_3) - 4\delta_2^2},$$

$$\xi_2^2 = -\frac{A_1(a_2 + a_3) - 2a_1\delta_2}{(a_2 + a_3)(A_2 + A_3) - 4\delta_2^2},$$

$$\eta_2 = \xi_1 = 0, \quad P_x = P_y = 0;$$

III. $$\eta_1^2 = -\frac{a_1(A_2 + A_3) - 2A_1(\delta_1 + \delta_2 - f^2\chi')}{(a_2 + a_3)(A_2 + A_3) - 4(\delta_1 + \delta_2 - f^2\chi')^2},$$

$$\xi_1^2 = -\frac{A_1(a_2 + a_3) - 2a_1(\delta_1 + \delta_2 - f^2\chi')}{(a_2 + a_3)(A_2 + A_3) - 4(\delta_1 + \delta_2 - f^2\chi')^2},$$

$$\eta_2 = \xi_2 = 0, \quad P_x = P_y = -f\chi'\eta_1\xi_1.$$

Phases I and II can be associated with the HT and LT phases, respectively, whereas phase III is an improper ferroelectric phase. Qualitative phase diagram for the discussed relations between the phenomenological coefficients is shown in figure 4(a). It can be shown that phase II appears in the phase diagram if $\Delta' = (a_2 + a_3)(A_2 + A_3) - 4\delta_2^2 > 0$. The lines 1

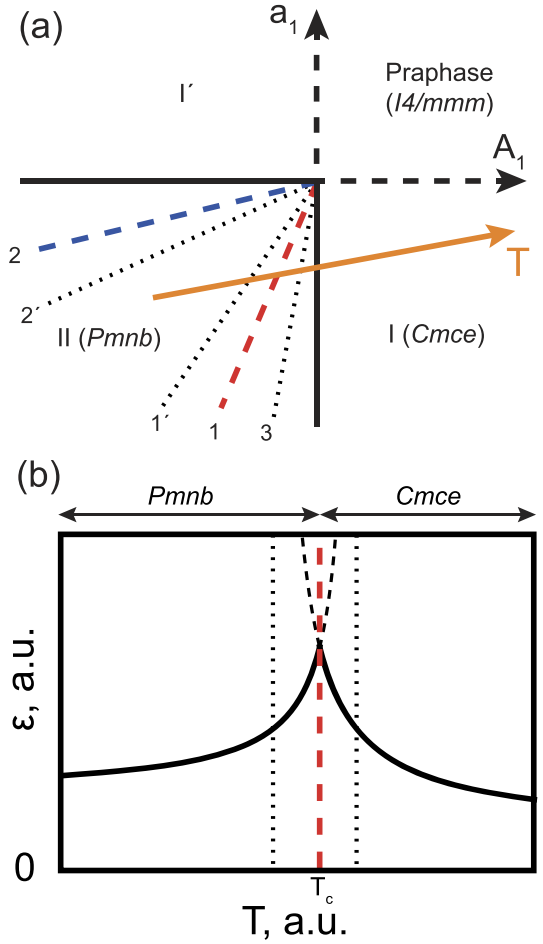

Figure 4. (a) Phase diagram for the model of phase transitions in $(i\text{-BA})_2CsPb_2Br_7$. Dashed lines are lines of second order phase transitions. Orange axis shows a possible temperature path. (b) Behavior of the dielectric constant along the temperature path shown in (a).

and 2 of second order phase transitions I–II and I′–II are given by equations

$$a_1 = \frac{a_2 + a_3}{2\delta_2}A_1, \tag{10}$$

$$a_1 = \frac{2\delta_2}{A_2 + A_3}A_1, \tag{11}$$

respectively. In turn, the lines 1′ and 2′ of would be (if the phase transitions I–II and I′–II had not occurred earlier) second order phase transitions I–III and I′–III are given by equations

$$a_1 = \frac{a_2 + a_3}{2(\delta_1 + \delta_2 - f^2\chi')}A_1, \tag{12}$$

$$a_1 = \frac{2(\delta_1 + \delta_2 - f^2\chi')}{A_2 + A_3}A_1, \tag{13}$$

respectively. Comparing (10) and (11) with (12) and (13) one finds that under the condition

$$\delta_1 - f^2\chi' > 0 \tag{14}$$

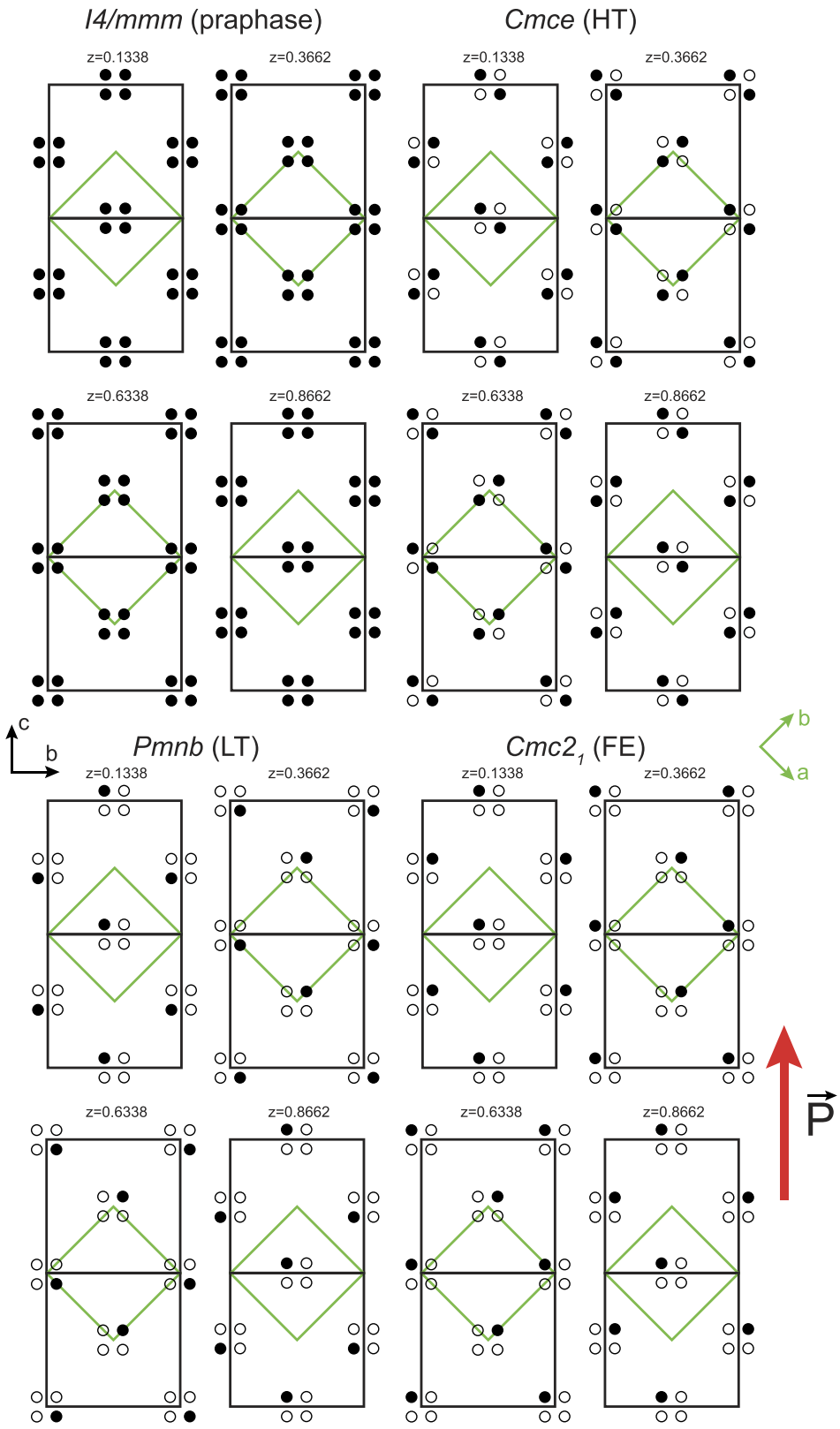

Figure 5. Schematic occupancies of nitrogen atomic positions in the praphase, HT, LT, and FE phases. Black unit cells correspond to those of the HT and LT phases. Green unit cell corresponds to the praphase structure. In the $I4/mmm$ structure each nitrogen is distributed over four available positions located around $(1/2, 1/2, 0.1338)$, $(0, 0, 0.3662)$, $(0, 0, 0.6338)$, and $(1/2, 1/2, 0.8662)$, which are shown by filled circles. In the HT phase two positions out of each four-positions set become empty (empty circles), whereas the other two are filled with equal probability. In the LT and FE structures nitrogen atoms occupy only one position in the four-positions sets. Red arrow shows the direction of electric polarization in the FE phase.

phase III is absent from the phase diagram and the phase transitions from phases I and I′ occur to the phase II as shown in figure 4(a).

The dielectric susceptibilities in phases I and II are given by

$$\chi^{\mathrm{I}}_{xx} = \chi^{\mathrm{I}}_{yy} = \chi' + \frac{a_1 f^2 \chi'^2}{2a_1(\delta_1 + \delta_2 - f^2\chi') - A_1(a_2 + a_3)},$$

$$\chi^{\mathrm{II}}_{xx} = \chi^{\mathrm{II}}_{yy} = \chi' + \chi_1 + \chi_2,$$

respectively, where

$$\chi_1 = \frac{a_1(A_2 + A_3) - 2A_1\delta_2}{c_1} f^2\chi'^2,$$

$$\chi_2 = \frac{A_1(a_2 + a_3) - 2a_1\delta_2}{c_2} f^2\chi'^2,$$

and

$$c_1 = 2\left[A_2\delta_2 + (A_2 + A_3)(\delta_1 - f^2\chi')\right] a_1 - A_1\left[A_2(a_2 + a_3) + 4\delta_2(\delta_1 - f^2\chi')\right],$$

$$c_2 = 2\left[a_2\delta_2 + (a_2 + a_3)(\delta_1 - f^2\chi')\right] A_1 - \left[a_2(A_2 + A_3) + 4\delta_2(\delta_1 - f^2\chi')\right] a_1.$$

It can be found that χ^{I}_{xx} and χ^{I}_{yy} diverge at line 1′ given by (12), whereas χ^{II}_{xx} and χ^{II}_{yy} diverge at the line determined by equation $c_1 = 0$ [line 3 in figure 4(a)]. Therefore, in good correspondence with the experimental data, qualitative behavior of the dielectric constant in the xy plane is as shown in figure 4(b). The phase transition I (HT)–II (LT) is between two centrosymmetric phases, however the dielectric constant experiences strong increase approaching the phase transition. It can be seen that the closer are the lines 1′ and 3 to line 1 the larger is the increase of the dielectric constant at the phase transition. In $(i\text{-BA})_2\mathrm{CsPb_2Br_7}$ the strongest and similar in values anomalies of the dielectric constant are experienced by ε_b and ε_c, i.e. the anomalies are in the bc plane of the *Cmce* structure, which corresponds to the xy plane of the tetragonal praphase in accordance with the present model.

In order to obtain qualitative results, in our model the expansion of the thermodynamic potential (8) is performed up to the fourth power with respect to OPs. This results in the second order I (HT)–II (LT) phase transition, whereas hysteretic behavior around T_c is experimentally observed, that may point to a more first order-like phase transition. Similar to the case of considering higher order terms in the thermodynamic potential expansion of model A in section 2.1, inclusion of higher order terms in the expansion (8) will allow for the corresponding theoretical description of the first order character of the phase transition in $(i\text{-BA})_2\mathrm{CsPb_2Br_7}$ as well as for the description of double hysteresis loops of electric polarization $P(E)$, however the results obtained in our simplified model will qualitatively remain the same.

3.3. The structure of the electric field-induced phase

The HT phase of $(i\text{-BA})_2\mathrm{CsPb_2Br_7}$ is characterized by disordered orientations of $i\text{-BA}^+$ cations, whereas at the HT–LT transition the ordering of their orientations occurs combined with antiparallel displacements of some other ions. External electric field applied in the LT phase results in the field-induced phase transition to a ferroelectric phase (FE) described by OPs (η_1, η_2) and (ξ_1, ξ_2) equal to $(\eta, 0)$ and $(\xi, 0)$ or, equivalently, to $(0, \eta)$ and $(0, \xi)$, respectively. According to the invariant (9), in the former case electric polarization is along the b-axis of the *Cmce* phase, whereas in the latter it is along the c-axis. It can be found that the space group symmetry of FE phase is $Cmc2_1$.

The analysis of occupational and displacement modes allows concluding on the orientations of $i\text{-BA}^+$ cations and ion displacements in the FE phase. Figure 5 shows the nitrogen occupancies in the praphase, HT, LT, and FE phases, which reflect the orientations of $i\text{-BA}^+$ cations. In the praphase there are four sets of four available positions for nitrogens and each position has occupancy 0.25 as depicted in figure 5(a). In the *Cmce* structure only two positions in each set are occupied with occupancy 0.5, whereas the other two positions are empty as shown in figure 5(b). In the *Pmnb* phase each nitrogen occupies only one position out of the two available in the *Cmce* structure. This ordering, shown in figure 5(c), occurs in a way that can be regarded as antiferroelectric ordering, at which different nitrogens occupy opposite positions. Detailed analysis of atomic displacements shows that this ordering is also accompanied by antiferroelectric atomic shifts. Figure 5(d) shows the ordering of nitrogens in the field-induced FE phase characterized by OPs $(0, \eta)$ and $(0, \xi)$. One can find that the occupied positions are aligned along the positive direction of axis c (here we refer to the *Cmce* or *Pmnb* structures), which is equivalent to the $[\bar{1}10]$ direction of the praphase. This results in appearance of electric polarization as shown in figure 5(d) in agreement with the interaction (9).

4. Discussion

In the present work we considered two models of phase transitions (models A and B), in which the dielectric constant experiences a strong increase across the phase transition between two centrosymmetric nonferroelectric phases. The main idea can be formulated as follows. A structural phase transition between two nonferroelectric phases can be described by one multicomponent or two single- or multicomponent order parameters, that induce improper ferroelectric phases. In the general case the complete phase diagram contains alternating nonferroelectric and improper ferroelectric phases. However, depending on the phenomenological coefficients of the thermodynamic potential expansion some phases can be absent from the phase diagram. Therefore, it is possible that a phase transition between two nonferroelectric phases occurs directly, although, however, in the general case this phase transition can be shown to occur through an intermediate improper ferroelectric phase. In this case, as we show in the models A and B, despite the fact that this intermediate improper

ferroelectric phase is hidden from the phase diagram, the dielectric constant experiences a strong increase at the phase transition between two centrosymmetric phases. In simple words, the closeness on thermodynamic path of the ferroelectric phase, either metastable or unstable, is felt by the system at the considered phase transition, which is reflected in the behavior of the dielectric constant across it.

Apart from the found dielectric behavior, the thermodynamic closeness of an improper ferroelectric phase to the phase transition between two nonferroelectric phases results in the fact that sufficiently strong external electric field should induce the hidden improper ferroelectric phase. At small electric fields the $P(E)$ dependence is essentially that of a paraelectric. However, above a certain critical field value the system should experience a field-induced transition to the ferroelectric phase accompanied by considerable growth of electric polarization. Therefore, upon approaching the considered structural phase transition and below it, the $P(E)$ dependence will experience double hysteresis loops characteristic for antiferroelectrics.

The interactions between the structural OPs and electric polarization that are responsible for improper ferroelectric behavior should be allowed by symmetry for structural OPs belonging to a wavevector with nonzero value. In the case that such structural distortions describe not, e.g. the rotations of oxygen octahedra, but cationic displacements, these will be essentially antiparallel displacements characteristic for antiferroelectrics. Therefore, the suggested models can be used for the design of antiferroelectric compounds by, e.g. synthesizing solid solutions of two compounds A and B that experience different structural instabilities that, acting together, can produce improper ferroelectric phases. The limiting cases $x = 0$ and $x = 1$ of such solid solution $A_{1-x}B_x$ will experience different structures described by $\eta \neq 0$ and $\xi \neq 0$, respectively. However, in general, at intermediate concentrations x close to the morphotropic phase boundary between the limiting cases one may expect that the improper ferroelectric phase induced by combination of structural instabilities η and ξ due to the coupling $\eta\xi P$ can be close on thermodynamic path resulting in antiferroelectric behavior.

The above ideas have been illustrated by the example of $(i\text{-BA})_2CsPb_2Br_7$, which experiences a structural phase transition at T_c between two centrosymmetric nonferroelectric phases and $P(E)$ double hysteresis loops below it. In the LT phase this compound experiences occupancies of available atomic sites, as well as atomic displacements in antiparallel fashion, characteristic of antiferroelectrics. According to our model, improper ferroelectric phase is thermodynamically close to the structural phase transition at T_c, which results in both considerable maximum of the dielectric constant at T_c and appearance of double hysteresis loops below this temperature.

As already mentioned in section 1 the continuing search for new ferroelectrics resulted in renewed interest in improper ferroelectricity. Under the name of the concept *hybrid improper ferroelectricity* within the last decade many compounds have shown to be ferroelectric due to simultaneous action of two or more structural nonpolar modes [8, 10, 16]. The corresponding interaction of structural modes with electric polarization is essentially that of model A studied in the present work. Here, therefore, we suggest that the improper ferroelectric mechanisms can be used for design of antiferroelectric compounds, because tailoring of compounds for simultaneous occurrence of structural modes that induce improper polarization is difficult and can result only in approaching the improper ferroelectric state but not reaching it. However, a state with a sufficiently close improper ferroelectric phase on the thermodynamic path can be of practical importance, because of appearance of double $P(E)$ loops and possible antiferroelectric-like antiparallel displacements of ions.

Finally, we would like to comment on the possibility of application of the proposed models to the prominent antiferroelectric $NaNbO_3$. The mode analysis of the two phases commonly observed in sodium niobate at room temperature, namely the Q and the P phases, was presented by Cochran and Zia [33]. Recently, a complete list of OPs that describe the phase transitions in $NaNbO_3$ has been found [34]. On cooling sodium niobate shows a high maximum of the dielectric constant and an about three-fold drop at the phase transition around 638 K between the phases with symmetries *Pmmn* (R phase) and *Pbcm* (P phase) [26]. In both crystal structures there is significant contribution from distortions characterized by wave vectors lying in the interior of the Brillouin zone and described by a six-dimensional IR T_4. In the R phase this mode belongs to the wave vector $\vec{k}_R = (1/2, 1/3, 1/2)$, whereas in the P phase to the vector $\vec{k}_P = (1/2, 1/2, 1/4)$. According to the INVARIANTS software [35, 36] IR T_4 in the $\vec{k}_R$ and $\vec{k}_P$ points induce 27 and 34 low symmetry phases out of which 12 and 17 are improper ferroelectric, respectively. Denoting $(m_1, m_2, m_3, m_4, m_5, m_6)$ and $(n_1, n_2, n_3, n_4, n_5, n_6)$ the OPs of the R and P phases, respectively, which transform according to T_4, we find the lowest order invariants responsible for improper ferroelectricity

$$m_5m_6(m_5^2 - 3m_6^2)(3m_5^2 - m_6^2)P_x + m_3m_4(m_3^2 - 3m_4^2) \times (3m_3^2 - m_4^2)P_y + m_1m_2(m_1^2 - 3m_2^2)(3m_1^2 - m_2^2)P_z, \tag{15}$$

and

$$n_5n_6(n_5^2 - n_6^2)P_x + n_3n_4(n_3^2 - n_4^2)P_y + n_1n_2(n_1^2 - n_2^2)P_z. \tag{16}$$

It can be seen that the invariant (16) is similar to that studied in model B, whereas the invariant (15) is of sixth power with respect to OP $\{m_i\}$, however all the results obtained for the model B should be still valid with minor changes. In the R phase the OP has the form $(0, 0, m, m/\sqrt{3}, 0, 0)$, whereas in the P phase it is $(n, n, 0, 0, 0, 0)$, which means that invariants (15) and (16) are equal to zero.

Experimental results including x-ray synchrotron, Raman spectroscopy, and transmission electron microscopy data evidence the appearance of incommensurate phases in both the P and R phase temperature regions [37–39]. The $\vec{k}_R$ and $\vec{k}_P$

points of the Brillouin zone are not special points along the line $(1/2, 1/2, \delta)$ and the locking of δ to commensurate values is determined, in particular, by anisotropy energy. Their successive appearance upon changes in temperature, as well as appearance of incommensurate δ values suggests that the anisotropy energy is small. Phenomenologically the appearance of incommensurate phases can be described by the Lifshitz invariants allowed for the OPs $\{n_i\}$ and $\{m_i\}$, which have the same form (here we write the invariant for $\{n_i\}$ only)

$$n_1\frac{\partial n_2}{\partial z} - n_2\frac{\partial n_1}{\partial z} + n_3\frac{\partial n_4}{\partial y} - n_4\frac{\partial n_3}{\partial y} + n_5\frac{\partial n_6}{\partial x} - n_6\frac{\partial n_5}{\partial x}.$$

The incommensurate phases will be characterized by spatially modulated OPs $(0, 0, m_3(y), m_4(y), 0, 0)$ and $(n_1(z), n_2(z), 0, 0, 0, 0)$ describing continuous rotation of OPs in the (m_3, m_4) and (n_1, n_2) planes, respectively. Such incommensurate phases are possible when the energy of anisotropy is low enough, which also means that the phase states with constant $m_3^2 \neq 3m_4^2$ $(3m_3^2 \neq m_4^2)$ and $n_3^2 \neq n_4^2$ have free energies comparable to those of phases R and P, respectively, and are thermodynamically close. However, according to invariants (15) and (16) such states are improper ferroelectric states. Therefore, according to model B, their closeness on thermodynamic path to the phases R and P should give considerable contribution to the dielectric constant of these phases.

In the R and P phases a ferroelectric phase should be induced by external electric field beyond some critical value, which will result in appearance of double $P(E)$ loops. Experimentally, however, it appears that in nominally pure $NaNbO_3$ after the ferroelectric phase has been induced by external field (the Q phase in the temperature region of the P phase), removal of electric field does not result in complete return to the initial phase due to the pinning of electric polarization. Moreover, slight variations in composition of $NaNbO_3$, appearance of defects, as well as different synthesis routes can result in emergence of the Q phase without application of electric field [40, 41].

5. Conclusions

In the present work we suggested two phenomenological models of a structural phase transition between centrosymmetric phases, that should be accompanied by a strong maximum of the dielectric constant. We show that this maximum is due to the thermodynamical closeness of a hidden improper ferroelectric phase. The validity of the models is illustrated by the recent example of a structural phase transition and antiferroelectric behavior of $((CH_3)_2CHCH_2NH_3)_2CsPb_2Br_7$. The results can be used for targeted design of antiferroelectric compounds, which experience different structural instabilities that, occurring simultaneously, induce improper ferroelectric phases.

Acknowledgments

The work was financially supported by the Russian Science Foundation grant No. 19-12-00205.

ORCID iDs

N V Ter-Oganessian https://orcid.org/0000-0001-8965-1800

References

[1] Levanyuk A P and Sannikov D G 1974 Improper ferroelectrics *Sov. Phys. Usp.* **17** 199
[2] Dvořák V 1974 Improper ferroelectrics *Ferroelectrics* **7** 1
[3] Sawada A and Takagi Y 1972 Mechanism of ferroelectric phase transition in ammonium Rochelle salt *J. Phys. Soc. Japan* **33** 1071
[4] Cross L E, Fouskova A and Cummins S E 1968 Gadolinium molybdate, a new type of ferroelectric crystal *Phys. Rev. Lett.* **21** 812
[5] Khomskii D 2009 Classifying multiferroics: mechanisms and effects *Physics* **2** 20
[6] Sakhennko V P and Ter-Oganessian N V 2010 Improper ferroelectric antiferromagnetics *Ferroelectrics* **400** 12
[7] Sakhnenko V P and Ter-Oganesyan N V 2003 Ferroelectric and ferroelastic phase states of crystals caused by atomic ordering *Crystallogr. Rep.* **48** 443
[8] Young J, Stroppa A, Picozzi S and Rondinelli J M 2015 Anharmonic lattice interactions in improper ferroelectrics for multiferroic design *J. Phys.: Condens. Matter* **27** 283202
[9] Benedek N A, Rondinelli J M, Djani H, Ghosez P and Lightfoot P 2015 Understanding ferroelectricity in layered perovskites: new ideas and insights from theory and experiments *Dalton Trans.* **44** 10543
[10] Benedek N A and Fennie C J 2011 Hybrid improper ferroelectricity: A mechanism for controllable polarization-magnetization coupling *Phys. Rev. Lett.* **106** 107204
[11] Clin M, Rivera J-P and Schmid. H 1990 Low temperature magnetoelectric effects on $Co_3B_7O_{13}I$ *Ferroelectrics* **108** 213
[12] Haque M S and Hardy J R 1980 Theoretical lattice-dynamical studies of the incommensurate phase transformation in K_2SeO_4 *Phys. Rev.* B **21** 245
[13] Perez-Mato J M, Gaztelua F, Madariaga G and Tello M J 1986 Symmetry-mode analysis of the ferroelectric phase in K_2SeO_4 *J. Phys. C: Solid State Phys.* **19** 1923
[14] Boullay P, Tellier J, Mercurio D, Manier M, Zuñiga F J and Perez-Mato J M 2012 Phase transition sequence in ferroelectric Aurivillius compounds investigated by single crystal x-ray diffraction *Solid State Sci.* **14** 1367
[15] Snedden A, Hervoches C H and Lightfoot P 2003 Ferroelectric phase transitions in $SrBi_2Nb_2O_9$ and $Bi_5Ti_3FeO_{15}$: a powder neutron diffraction study *Phys. Rev.* B **67** 092102
[16] Benedek N A 2014 Origin of ferroelectricity in a family of polar oxides: the Dion-Jacobson phases *Inorg. Chem.* **53** 3769
[17] Liu Z, Lu T, Ye J, Wang G, Dong X, Withers R and Liu Y 2018 Antiferroelectrics for energy storage applications: a review *Adv. Mater. Technol.* **3** 1800111
[18] Pan W, Zhang Q, Bhalla A and Cross L E 1989 Field-forced antiferroelectric-to-ferroelectric switching in modified lead zirconate titanate stannate ceramics *J. Am. Ceram. Soc.* **72** 571
[19] Shimizu H, Guo H, Reyes-Lillo S E, Mizuno Y, Rabe K M and Randall C A 2015 Lead-free antiferroelectric: xCaZrO$_3$-(1-x)NaNbO$_3$ system ($0 \leqslant x \leqslant 0.10$) *Dalton Trans.* **44** 10763

[20] Tan X, Xu Z, Liu X and Fan Z 2018 Double hysteresis loops at room temperature in $NaNbO_3$-based lead-free antiferroelectric ceramics *Mater. Res. Lett.* **6** 159

[21] Guo H, Shimizu H, Mizuno Y and Randall C A 2015 Strategy for stabilization of the antiferroelectric phase (*Pbma*) over the metastable ferroelectric phase ($P2_1ma$) to establish double loop hysteresis in lead-free (1-*x*)$NaNbO_3$-*x*$SrZrO_3$ solid solution *J. Appl. Phys.* **117** 214103

[22] Gao L, Guo H, Zhang S and Randall C A 2016 A perovskite lead-free antiferroelectric *x*$CaHfO_3$-(1-*x*)$NaNbO_3$ with induced double hysteresis loops at room temperature *J. Appl. Phys.* **120** 204102

[23] Tian Y, Jin L, Zhang H, Xu Z, Wei X, Viola G, Abrahams I and Yan H 2017 Phase transitions in bismuth-modified silver niobate ceramics for high power energy storage *J. Mater. Chem.* A **5** 17525

[24] Zhao L, Gao J, Liu Q, Zhang S and Li J-F 2018 Silver niobate lead-free antiferroelectric ceramics: enhancing energy storage density by *B*-site doping *ACS Appl. Mater. Interfaces* **10** 819

[25] Zhao L, Liu Q, Gao J, Zhang S and Li J-F 2017 Lead-free antiferroelectric silver niobate tantalate with high energy storage performance *Adv. Mater.* **29** 1701824

[26] Mishra S K, Choudhury N, Chaplot S L, Krishna P S R and Mittal. R 2007 Competing antiferroelectric and ferroelectric interactions in $NaNbO_3$: neutron diffraction and theoretical studies *Phys. Rev.* B **76** 024110

[27] Sciau P, Kania A, Dkhil B, Suard E and Ratuszna A 2004 Structural investigation of $AgNbO_3$ phases using x-ray and neutron diffraction *J. Phys.: Condens. Matter* **16** 2795

[28] Albers J, Klöpperpieper A, Rother H J and Ehses K H 1982 Antiferroelectricity in betaine phosphate *Phys. Status Solidi a* **74** 553

[29] Wu Z, Liu X, Ji C, Li L, Wang S, Peng Y, Tao K, Sun Z, Hong M and Luo J 2019 Discovery of an above-room-temperature antiferroelectric in two-dimensional hybrid perovskite *J. Am. Chem. Soc.* **141** 3812

[30] Tolédano J-C and Tolédano P 1987 *The Landau Theory of Phase Transitions* (Singapore: World Scientific)

[31] Sakhnenko V P and Ter-Oganessian N V 2012 Praphase concept for the phenomenological description of magnetoelectrics *Crystallogr. Rep.* **57** 112

[32] Ter-Oganessian N V and Sakhnenko V P 2014 Interpretation of magnetoelectric phase states using the praphase concept and exchange symmetry *J. Phys.: Condens. Matter.* **26** 036003

[33] Cochran W and Zia A 1968 Structure and dynamics of perovskite-like crystals *Phys. Status Solidi b* **25** 273

[34] Tolédano P and Khalyavin D D 2019 Symmetry-determined antiferroelectricity in $PbZrO_3$, $NaNbO_3$, and $PbHfO_3$ *Phys. Rev.* B **99** 024105

[35] Stokes H T, Hatch D M and Campbell B J 2019 *INVARIANTS,* ISOTROPY Software Suite iso.byu.edu

[36] Hatch D M and Stokes H T 2003 INVARIANTS: program for obtaining a list of invariant polynomials of the order parameter components associated with irreducible representations of a space group *J. Appl. Crystallogr.* **36** 951

[37] Reznichenko L A, Shilkina L A, Gagarina E S, Raevskii I P, Dul'kin E A, Kuznetsova E M and Akhnazarova V V 2003 Structural instabilities, incommensurate modulations and P and Q phases in sodium niobate in the temperature range 300–500 K *Crystallogr. Rep.* **48** 448

[38] Yuzyuk Y I, Simon P, Gagarina E, Hennet L, Thiaudiére D, Torgashev V I, Raevskaya S I, Raevskii I P, Reznitchenko L A and Sauvajol J L 2005 Modulated phases in $NaNbO_3$: Raman scattering, synchrotron x-ray diffraction, and dielectric investigations *J. Phys.: Condens. Matter* **17** 4977

[39] Guo H, Shimizu H and Randall C A 2015 Direct evidence of an incommensurate phase in $NaNbO_3$ and its implication in $NaNbO_3$-based lead-free antiferroelectrics *Appl. Phys. Lett.* **107** 112904

[40] Chen J and Feng D 1988 TEM study of phases and domains in $NaNbO_3$ at room temperature *Phys. Status Solidi b* **109** 171

[41] Chen J and Feng D 1988 In situ TEM studies of para–ferro phase transitions in $NaNbO_3$ *Phys. Status Solidi a* **109** 427